Geophysical Journal International

Geophys. J. Int. (2009) **179,** 1566–1572 doi: 10.1111/j.1365-246X.2009.04389.x

FAST TRACK PAPER

Detecting the limit of slab break-off in central Turkey: new high-resolution *Pn* tomography results

Christine R. Gans,[1] Susan L. Beck,[1] George Zandt,[1] C. Berk Biryol[1] and A. Arda Ozacar[2]

[1]*Department of Geosciences, University of Arizona, Tucson,* AZ 85721, *USA. E-mail: cgans@email.arizona.edu*
[2]*Department of Geological Engineering, Middle East Technical University, Ankara, Turkey* 06531

Accepted 2009 September 16. Received 2009 September 9; in original form 2009 February 11

SUMMARY

Inversion of *Pn* traveltime residuals from a 39-station broad-band array provides a high-resolution image of the velocity structure in the uppermost mantle beneath central Turkey. Individually picked *Pn* phase arrivals from events recorded by the North Anatolian Fault Passive Seismic Experiment and the Kandilli Observatory were combined with additional events associated with the Eastern Turkey Seismic Experiment. Tomography results show no change in *Pn* velocity across the North Anatolian Fault, although longitudinal variations are evident. A region of very low *Pn* velocities ($<$7.8 km s^{-1}) is imaged east of the Central Anatolian Fault Zone (CAFZ), with a transition to faster velocities ($>$8.1 km s^{-1}) west of the fault. The sharp transition along the CAFZ, which follows the palaeotectonic Inner-Tauride Suture, may represent the location of the edge of the slab window, created when the oceanic slab broke off along the Bitlis-Zagros Suture around 11 Ma, as the Arabian plate collided with the Eurasian plate.

Key words: Interface waves; Seismic tomography; Continental margins: transform; Asia.

GJI Seismology

INTRODUCTION

Turkey is part of a tectonically active region, with large earthquakes commonly occurring on its major fault zones, including the North Anatolian (NAFZ) and the East Anatolian Fault Zones (EAFZ) (Fig. 1). Central and western Turkey are part of the Anatolian Plate, which is currently rotating counter-clockwise with increasing velocities from east to west (in a Eurasian reference frame) at ∼18 to 25 mm yr^{-1} (Reilinger *et al.* 2006). Whether the westward motion of this Anatolia block is due to escape tectonics (Tapponnier 1977) or slab rollback (Reilinger *et al.* 2006) is still controversial. What is known is that this motion is being accommodated on both the NAFZ and EAFZ, as evidenced by the many large and destructive earthquakes. Total offset on the dextral, east to west propagating North Anatolian Fault (NAF) is estimated at ∼100 to 20 km, respectively (Sengör *et al.* 2005). The sinistral EAFZ has much less offset. While the cumulative offset is still under debate, most estimates vary from ∼5 to 25 km, with one as high as ∼40 km (Bozkurt 2001 and references therein). The sinistral Central Anatolian Fault Zone (CAFZ), located to the northwest of the EAFZ, is seismically less active, yet it has been suggested that it will eventually replace the EAFZ as the eastern boundary of the Anatolian Plate (Kocyigit & Beyhan 1998).

Building on the slab steepening and break-off model for the eastern Anatolian Plateau by Keskin (2003), Faccenna *et al.* (2006) have proposed the existence of a continuous (oceanic) subducting slab that extended from the Hellenic trench to the Bitlis region, which was subsequently torn during slab break-off after the Arabian Plate collided with the Eurasian Plate at the Bitlis-Zagros Suture. Based on their experiments, the westward escape of Anatolia and the formation of the NAFZ can be explained by a combination of the Arabian collision and slab retreat along the Hellenic trench. They were unable, however, to determine the location of the slab rupture edge. We propose in this study that the downdip limit of the slab window, caused by the break-off of the Arabian slab at 11 Ma, occurs along the CAFZ and continues to the west, as imaged using high-resolution *Pn* tomography.

In order to understand present day tectonics, a brief overview of the tectonic history of central Turkey is necessary. Multiple phases of ocean basin formation and closure have occurred since the Permian (Sengör & Yilmaz 1981), leading to an amalgamation of oceanic, volcanic and metamorphic rocks separated by a number of suture zones (Fig. 1). In central Turkey, the Inner-Tauride Suture (ITS) separates the Cretaceous metamorphic and granitic rocks of the Kirsehir Massif from the Anatolide-Tauride Block (e.g. Sengör & Yilmaz 1981; Okay & Tüysüz 1999). The $>$700-km-long CAFZ

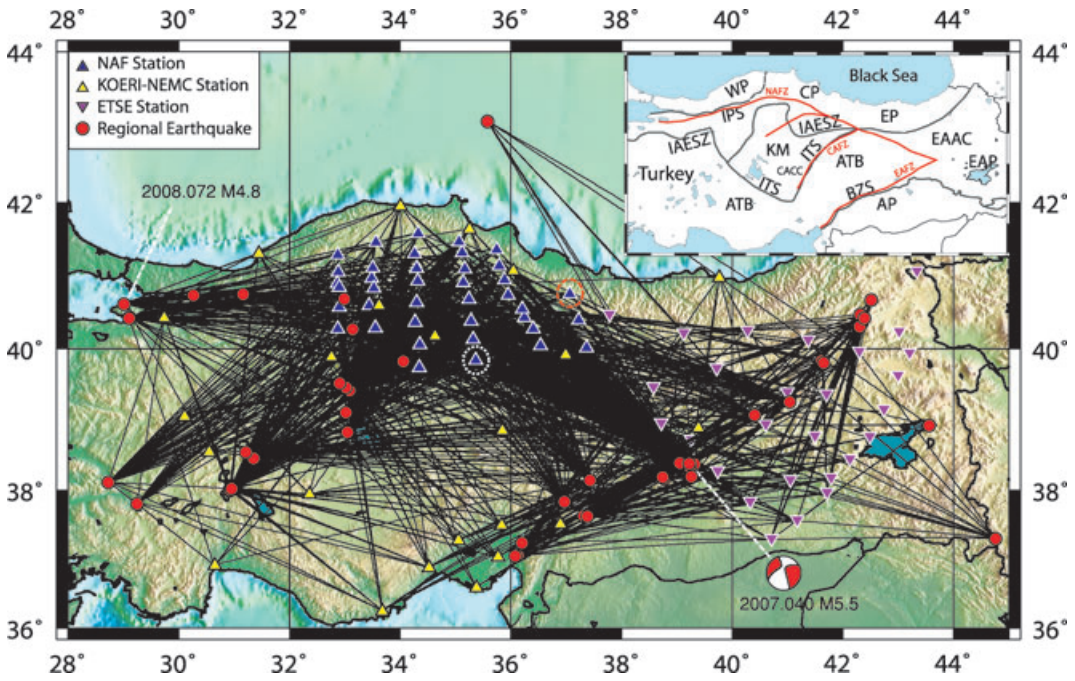

Figure 1. Map of study area with locations of stations (triangles) and events (solid red circles). Lines are the station-event paths used in the inversion. White dotted circle shows station INSU, red dashed circle station ISKE (see Fig. 2). Inset shows major tectonic features and sutures, with major faults shown in red (modified after Keskin *et al.* 2008). IPS – Intra-Pontide Suture, IAESZ – Izmir-Ankara-Erzincan Suture Zone, ITS – Inner-Tauride Suture, BZS – Bitlis-Zagros Suture, EAAC – Eastern Anatolian Accretionary Complex, CACC – Central Anatolian Crystalline Complex, ATB – Anatolide-Tauride Block, KM – Kirsehir Massif, WP – Western Pontides, CP – Central Pontides, EP – Eastern Pontides, AP – Arabian Platform, NAFZ – North Anatolian Fault Zone, CAFZ – Central Anatolian Fault Zone, EAFZ – East Anatolian Fault Zone, EAP – Eastern Anatolian Plateau.

follows the older ITS, and was reactivated in the middle Pliocene (Kocyigit & Beyhan 1998). The ITS forms the eastern boundary of the Central Anatolian Crystalline Complex (CACC) (Whitney *et al.* 2007), and may play an important role in the escape tectonics of central and western Turkey (Kocyigit & Beyhan 1998; Dirik 2001). In northern Turkey, the continental basement material of the Pontides is separated from the Kirsehir Massif and the Anatolide-Tauride Block by the ∼2000 km long Palaeocene Izmir-Ankara-Erzincan Suture Zone (IAESZ) (Okay & Tüysüz 1999). The ∼800-km-long Intra-Pontide Suture (IPS), formed during the early Eocene, is associated with the opening of the western Black Sea basin.

The NAFZ, which initiated in the east between 13 and 11 Ma and subsequently propagated westward, follows the path of the IPS (e.g. Sengör *et al.* 2005). The 1400-km-long dextral strike-slip fault is seismically active and capable of large, destructive earthquakes (e.g. Sengör *et al.* 2005). The NAF Passive Seismic Experiment (2005–2008), a joint project between the University of Arizona, Middle East Technical University, Istanbul Technical University and Bogazici University Kandilli Observatory, recorded data from 39 broadband seismometers (Fig. 1). Using regional earthquakes from this experiment, as well as others from the Eastern Turkey Seismic Experiment (ETSE, 1999–2001) (Sandvol *et al.* 2003), we picked over 1300 *Pn* phases in order to investigate the velocity structure of the uppermost mantle. The *Pn* phase is a compressional wave that travels through the crust, refracts into the mantle, and then propagates through the mantle lid at mantle velocities. *Pn* traveltime residuals were inverted for *Pn*-wave velocity beneath central Turkey, providing a new, higher-resolution image than has been previously published (Al-Lazki *et al.* 2003, 2004) for this region.

Pn INVERSION METHOD

Data from both the NAF Passive Seismic Experiment and the ETSE were used in the inversion. Initially, we looked at 24 regional earthquakes that occurred during the NAF experiment, located from 1.8° to 10° from a station. While the *Pn* phase is the initial arrival up to 16°, beyond ∼10° the signal was generally considered too noisy to pick an accurate phase onset. For each of these earthquakes, we added data from stations of the Kandilli Observatory and Earthquake Research Institute and National Earthquake Monitoring Center (KOERI-NEMC) network, where available (Fig. 1). Earthquake locations and origin times are from the KOERI-NEMC earthquake catalogue. In order to expand our coverage and increase resolution to the east, we then incorporated 23 additional regional earthquakes that occurred during the ETSE deployment. Overall, more than 1300 *Pn* phases were individually identified and incorporated into the inversion. Error on the arrival picks is estimated to be ∼0.1 s. Ray paths are shown in Fig. 1, with sample vertical component records from two earthquakes shown in Fig. 2.

Using the tomography method of Hearn (1996), traveltime residuals were inverted to obtain the *Pn* velocity for the uppermost mantle. The traveltime path contains three legs: event, mantle and station, and is described by the traveltime equation

$$t_{ij} = a_i + b_j + \sum d_{ijk}(s_k), \qquad (1)$$

where a_i is the station time leg for station i, b_j is the event time leg for event j, d_{ijk} is the distance between event j and station i for cell k, and s_k is the slowness perturbation for cell k (Hearn 1984, 1996). In this method, a least squares algorithm (Paige & Saunders 1982) iteratively solves for all event-station pairs to find slowness (s_k), station (a_i), and event (b_j) delays. For this study we did not solve

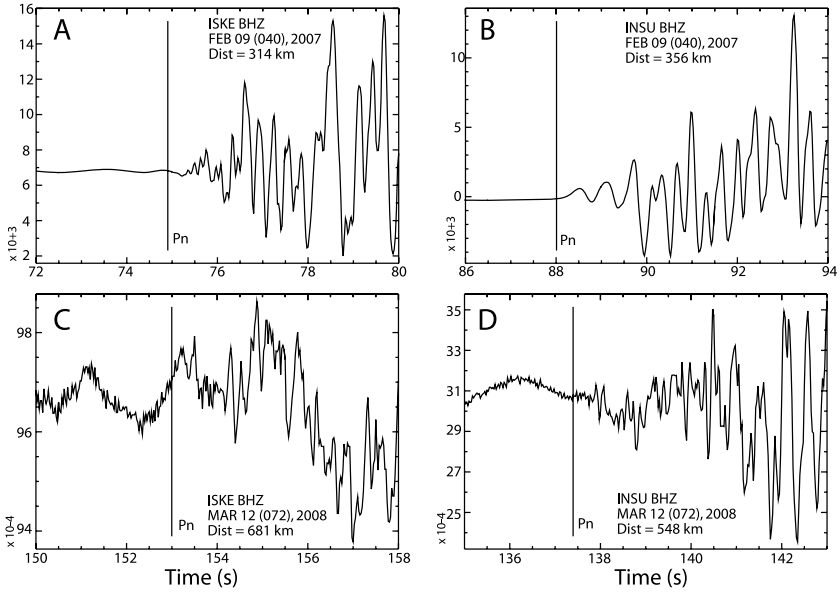

Figure 2. Sample vertical component records with *Pn* arrivals marked. (a,b) Event on 2007.040 (M5.5) with clean easy-to-pick arrivals. (c, d) Event on 2008.072 (M4.8) with nosier harder-to-pick arrivals. Station locations are shown in Fig. 1. The *Pn* phase is often small and emergent (a and c), making it important to have accurate picks.

for anisotropy, and so those terms are not included in the traveltime equation. Using an assumed crustal model (35 km crustal thickness with a velocity of 6.2 km s^{-1}) and an average *Pn* velocity from the study area (7.9 km s^{-1} as determined by the linear fit to the slope of the traveltime data), the traveltimes for each station and event leg were separated. Varying crustal thickness by up to 10 km did not significantly change results. For the inversion, a cell size of 0.25° × 0.25° was used. Further, a Laplacian damping factor was applied to regularize the solution (Paige & Saunders 1982; Hearn 1996). Higher damping gives lower estimated parameter errors and reduces the noise artefacts, but increases the resolution width. Lower damping increases both the parameter errors and the range of velocity variations. Due to the high accuracy of our hand-picked *Pn* arrivals (in contrast to automated picks sometimes used in previous studies), we chose a lower damping value of 200, which provided acceptably low errors while keeping the model perturbations reasonably small (inset, Fig. 3). Further, we required a minimum of six arrivals per cell; those not meeting this requirement were shaded grey (Figs 3 and 4).

RESOLUTION ANALYSIS

We performed an inversion on a synthetic checkerboard model to test the resolution of our *Pn* velocity inversion. The checkerboard contained cells of varying sizes with alternating ±0.25 km s^{-1} velocities and 0.1 s added random noise. By hand picking our data, with estimated errors on the order of ∼0.1 s, we assumed random noise was much smaller than the 'noise' produced by structural complexity. The inversion was then run using the same station and event distribution, and damping, used in the *Pn* tomography, with the edge of the checkerboard centred on 41° N, approximating a contrast along the NAFZ. Resolution is very good with 2° cells (Fig. 3), but still reasonable with 1.5°. Below this, reproducibility is poor. As shown in Fig. 3, amplitudes are recovered very well in the region of the NAF experiment, as well as to the east around the western portion of the ETSE experiment. While we lose some amplitude recovery at the edges of our grid and to the south, we do have sufficient coverage to recognize a contrast across the NAFZ of 0.25 km s^{-1} or larger, although our east–west resolution north of the fault is poor.

Our *Pn* tomographic inversion shows a 77 per cent variance reduction from the input linear-fit traveltime residuals (Fig. 3). The standard deviations for the velocity cells of the model can be found in Fig. S1. We used 100 bootstrap iterations to calculate solution variances (Koch 1992; Hearn & Ni 1994). The average standard deviation of the velocity perturbations is 0.05 km s^{-1}; within the area of interest most cells average less than 0.025 km s^{-1}. Crustal station delays for the region are small; negative delays average −0.31 s and positive average 0.27 s. Standard deviations of the station delays are also very small, averaging 0.19 s. Both of these figures can be found in Fig. S2.

RESULTS

Most striking from the inversion results is the zone of very low *Pn* velocities (<7.8 km s^{-1}) located in eastern Turkey, on the Turkish/Anatolian Plateau (Fig. 4). This slow region was also imaged by Al-Lazki *et al.* (2003, 2004) using data from, among others, the ETSE deployment. They hypothesized that this zone lacks a mantle lid, based on their *Pn* tomography results, as well as the strong Sn attenuation in the area (Gök *et al.* 2003). Our results from the NAF experiment show a zone of faster (>8.1 km s^{-1}) *Pn* velocities located beneath the Cankiri and Safranbolu Basins (Fig. 4), regions underlain by basement massifs (e.g. Kaymakci *et al.* 2003; Keskin *et al.* 2008). Higher *Pn* velocities are often linked to regions with stable continental blocks, such as the Kirsehir Massif and the CACC (e.g. Hearn & Ni 1994; Al-Lazki *et al.* 2003). This zone of higher velocities appears to cross tectonic belts, the NAFZ, and the IPS. Previously published *Pn* tomography results for this region, however, show slower velocities in this area (Al-Lazki *et al.* 2004), opposite to our findings. Further, there is a distinct (and previously undetected) transition between the faster and slower zones, which appears to follow the northern portion of the active sinistral CAFZ (Kocyigit & Beyhan 1998), a region associated with the

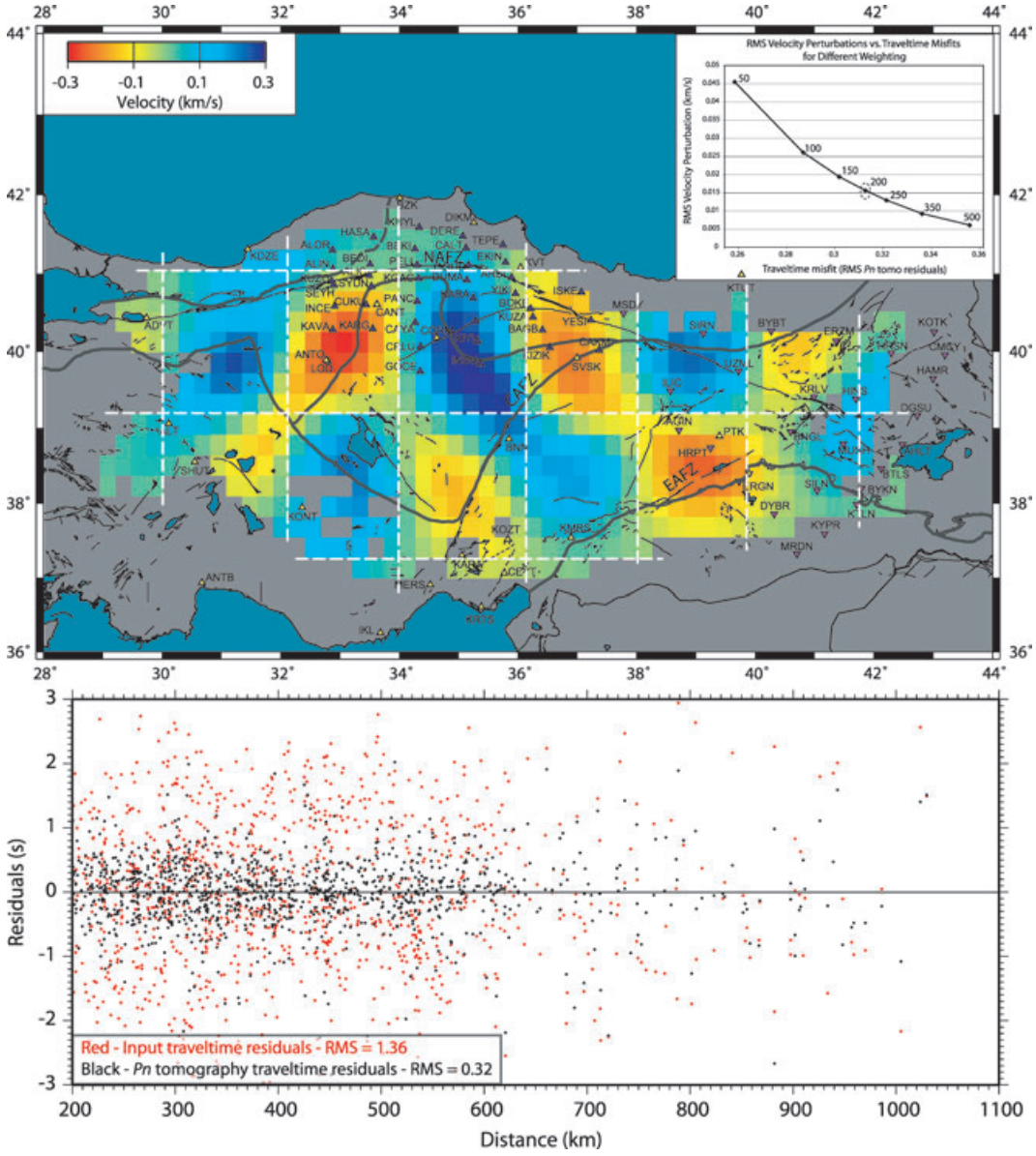

Figure 3. Top: Checkerboard test results for 2° cells using the same station and event paths as in the *Pn* tomography, with 0.1 s random noise added. The transition is centred on 41°N, with 100 bootstrap iterations. Dashed white lines indicate approximate outline of checkerboard cell size. Inset: Root Mean Square (RMS) velocity perturbations versus traveltime misfits (RMS final *Pn* tomography residuals) for various weight/damping values. We chose a damping parameter of 200 for our study. Stations and sutures are as in Fig. 1. NAFZ – North Anatolian Fault Zone, CAFZ – Central Anatolian Fault Zone, EAFZ – East Anatolian Fault Zone Bottom: Input traveltime residuals (red), calculated using the average *Pn* velocity (7.9 km s^{-1}) for the study area, versus residuals calculated using our *Pn* tomography results. There is a 77 per cent variance reduction obtained using the inversion.

Palaeotectonic ITS. This strong upper mantle signature was initially imaged using only data from the NAF and KOERI-NEMC networks, but persisted when data from the ETSE deployment was included, increasing our confidence in the location of this transition from faster to slower *Pn* velocities across the CAFZ. This transition also corresponds to a change in the Bouguer gravity anomaly from higher (∼−60 mGal) west of the CAFZ to lower (∼−100 mGal) to the east (inset, Fig. 4; Ates *et al.* 1999). The southern termination of this low-velocity zone (near 38°N and 36° E) also corresponds to a profound topographic and gravimetric boundary consistent with denser lower crust and upper mantle to the south. The lower *Pn* velocities at the southern limit of the CAFZ, which occur west of the fault, are consistent with the presence of young volcanics in this region (Fig. 4, Whitney *et al.* 2007). At the edge of our resolution area, we also image a zone of faster *Pn* velocities south of the Bitlis-Zagros Suture, which likely represents the Arabian mantle lid (Al-Lazki *et al.* 2003) and the edge of slab break-off. Although it is also on the edge of our well-resolved area, there is a ridge of high *Pn* velocity that separates the low-*Pn* anomalies beneath Eastern Anatolia and the western low-velocity anomaly located between the Central and Eastern Anatolian Fault Zones. The Eastern Anatolian Plateau (Inset, Fig. 1) is a dome-shaped topographic high centred on Lake Van and is characterized by extensive young volcanic cover related to a southward sweep of volcanism associated with slab steepening and break-off (Keskin 2003). We note that the western edge of this Neogene volcanic province approximately coincides with the zone of high *Pn* velocity, perhaps indicating that the high velocity feature is a ridge or finger of

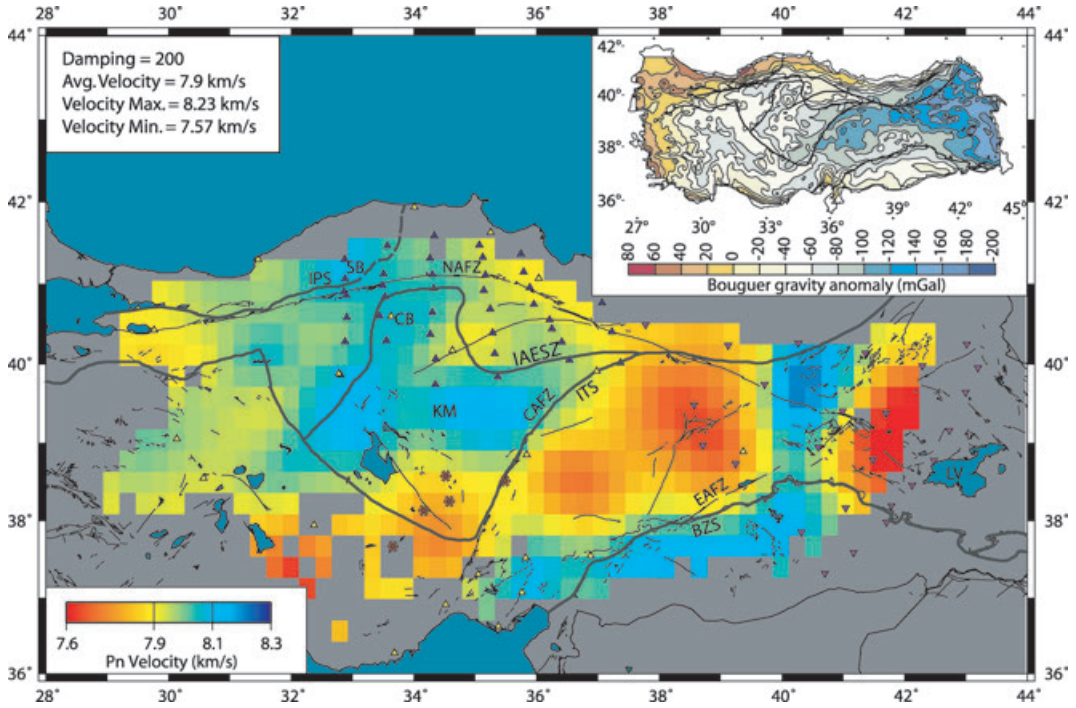

Figure 4. Pn tomography results for north-central Turkey. Stations and sutures are as in Fig. 1. NAFZ – North Anatolian Fault Zone, CAFZ – Central Anatolian Fault Zone, EAFZ – East Anatolian Fault Zone, KM – Kirsehir massif, SB – Safranbolu Basin, CB – Cankiri Basin, LV – Lake Van. Red asterisks are Holocene volcanoes. Inset: Bouguer gravity anomaly map of Turkey (from Ates *et al.* 1999).

subducted lithosphere that remained in place (Fig. 5). The central axis of the NE–SW oriented western low-velocity anomaly is located beneath the Elazig–Malatya–Kahramanmaras volcanics, ranging in age from Miocene to Quaternary (Kürüm *et al.* 2008). The correlation of the location of these young volcanic fields with areas of low *Pn* velocities supports models that relate this volcanism to upper mantle processes.

Another important finding is the lack of contrast in *Pn* velocity across the NAFZ. Traveling east to west, *Pn* velocities found in the Eastern Pontides are initially slower, increase into the Central Pontides, and then decrease again somewhat in the westernmost Western Pontides. There do not appear to be significant latitudinal variations across the NAFZ west of 35° E (Fig. 4).

DISCUSSION AND CONCLUSIONS

While *Pn* velocities vary east to west along the NAFZ, there is no observable variation in *Pn* velocity north versus south of the NAFZ, as has been observed in Bouguer gravity anomalies (lower anomalies south of the fault versus higher to the north) (inset, Fig. 4; Ates *et al.* 1999). The positive gravity signal around the NAFZ could be due to crustal thinning at the edge of the Black Sea coastline, about 150 km further north, which parallels the NAFZ. If so, the longer wavelength of this gravity signal could produce an apparent correlation with the NAFZ. Further, SKS results do not show a change in orientation or lag time across the NAFZ, implying the lack of a deep-seated signature for the NAFZ (Biryol *et al.* 2008). We find an absence of variation in *Pn* velocity across the NAFZ, which could be due to a number of reasons, including that nothing is being offset in the mantle, or perhaps that the fault does not penetrate vertically into the mantle.

Whereas the seismically active NAFZ shows no upper mantle signature across the fault, the less-active CAFZ has an exceptionally distinct one. The transition in *Pn* velocities across the CAFZ is very discrete, and could represent the edge of the region of upwelled asthenosphere (Fig. 5). This slab window resulted from the Arabian slab detachment, proposed by multiple authors for easternmost Turkey along the Bitlis-Zagros Suture (Keskin 2003; Faccenna *et al.* 2006; Lei & Zhao 2007; Elitok & Dolmaz 2008; Gögüs & Pysklywec 2008). The oceanic slab is thought to have detached around 11–10 Ma, causing the hot asthenosphere to rise and come in contact with the continental lithosphere (Keskin 2003; Sengör *et al.* 2003). This slab detachment or break-off has been proposed as a cause for the initiation of the NAFZ (Faccenna *et al.* 2006). Our region of very low *Pn* velocity to the east of the CAFZ corresponds to the region suggested by Al-Lazki *et al.* (2003, 2004) to contain little or no mantle lid. The gravity low that is observed south and east of the CAFZ corresponds to our transition from fast to slow *Pn* velocities. This negative anomaly (∼−100 mGal) might be explained by a thin mantle lid in this region, which would bring lower density material (i.e. hot asthenosphere) closer to the surface, through a slab window. With the improved resolution in our study, we are able to distinguish a western and eastern part of this anomaly. The eastern portion corresponds to the highest elevations of the Eastern Anatolian Plateau and the most voluminous Miocene to Quaternary volcanism, whereas the western portion, which is in part bounded by the CAFZ, corresponds to a slightly lower average elevation and less voluminous volcanism.

Fig. 5 shows a cartoon, based on Faccenna *et al.* (2006), of our proposed geometry of slab break-off beneath eastern and central Anatolia. The break-off of the oceanic lithosphere from the Arabian continental lithosphere downdip of the collision zone appears to have propagated westward, beyond the edge of the Arabian platform. Complicating this picture is a ridge of still-intact high *Pn* velocity at the 'nose' of the Bitlis suture zone. Our data does not constrain whether this is a piece of oceanic slab, as depicted in the figure, or

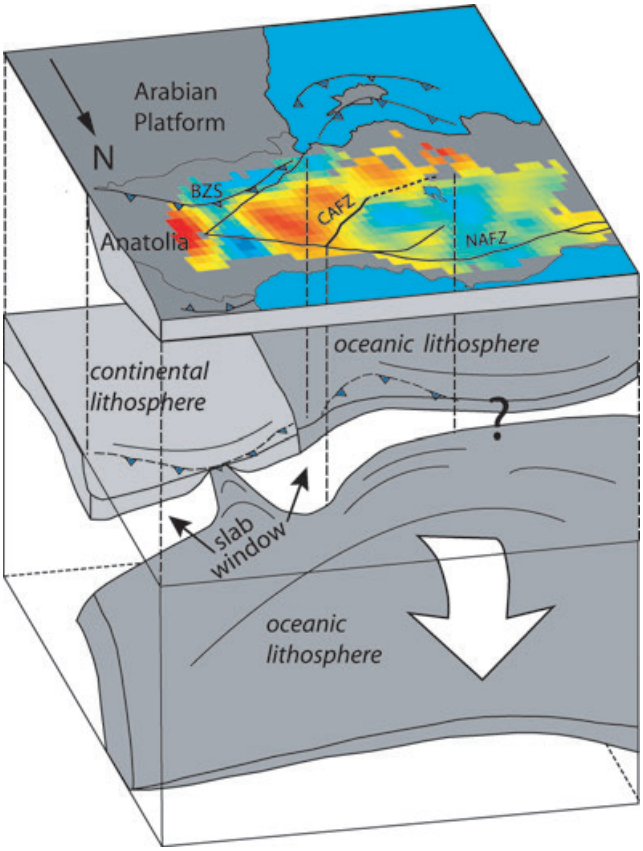

Figure 5. Cartoon showing hypothesized upper mantle slab detachment and resulting slab window consistent with *Pn* tomography results. The downdip edge of the slab window corresponds to the northern edge of the low *Pn* region that partially follows the CAFZ. The western extent of the tear is uncertain. Modified after Faccenna *et al.* (2006).

a promontory of continental lithosphere. In either case, the ridge separates the opening slab window into eastern and western parts that appear to have different surface volcanic expressions. To the west, the transition from faster to slower *Pn* velocities along the CAFZ could mark the previously unrecognized northwest limit of the slab window in this region, providing constraints on the model of Faccenna *et al.* (2006).

ACKNOWLEDGMENTS

This experiment would not have been possible without the support of our Turkish collaborators: N. Turkelli, T. Taymaz, A. Kocygit, E. Bozkurt and H. Tok. We thank T. Hearn for generously lending us his tomography code. Our resolution was improved with the addition of data made available by the KOERI-NEMC. This manuscript was improved by the thorough review of Frederik Tilmann. We are grateful to IRIS and people at the PASSCAL Instrument Center for their help and support throughout the NAF deployment. The seismic instruments were provided by the Incorporated Research Institutions for Seismology (IRIS) through the PASSCAL Instrument Center (NSF Cooperative Agreement EAR-0552316). This research was supported by the National Science Foundation (EAR0309838). Maps were created using the Generic Mapping Tools (GMT) software (Wessel & Smith 1998).

REFERENCES

Al-Lazki, A.I., Seber, D., Sandvol, E., Turkelli, N., Mohamad, R. & Barazangi, M., 2003. Tomographic Pn velocity and anisotropy structure beneath the Anatolian plateau (eastern Turkey) and the surrounding regions, *Geophys. Res. Lett.,* **30**(24), 8043, doi:10.1029/2003GL017391.

Al-Lazki, A.I., Sandvol, E., Seber, D., Barazangi, M., Turkelli, N. & Mohamad, R., 2004. *Pn* tomographic imaging of mantle lid velocity and anisotropy at the junction of the Arabian, Eurasian and African plates, *Geophys. J. Int.,* **158,** 1024–1040.

Ates, A., Kearey, P. & Tufan, S., 1999. New gravity and magnetic anomaly maps of Turkey, *Geophys. J. Int.,* **136,** 499–502.

Biryol, C.B. *et al*., 2008. NAF Experiment: Seismic Anisotropy Beneath Northern Anatolia From Shear-Wave Splitting, *EOS, Trans. Am. Geophys. Un.,* **89**(53), Fall Meet. Suppl., Abstract T21A-1916.

Bozkurt, E., 2001. Neotectonics of Turkey – a synthesis, *Geodin. Acta,* **14,** 3–30.

Dirik, K., 2001. Neotectonic evolution of the northwestward arched segment of the Central Anatolian Fault Zone, Central Anatolia, Turkey, *Geodinamica Acta,* **14,** 147–158.

Elitok, Ö. & Dolmaz, M.N., 2008. Mantle flow-induced crustal thinning in the area between the easternmost part of the Anatolian plate and the Arabian Foreland (E Turkey) deduced from the geological and geophysical data, *Gondwana Res.,* **13,** 302–318.

Faccenna, C., Bellier, O., Martinod, J., Piromallo, C. & Regard, V., 2006. Slab detachment beneath eastern Anatolia: a possible cause for the formation of the North Anatolian fault, *Earth planet. Sci. Lett.,* **242,** 85–97.

Gögüs, O.H. & Pysklywec, R.N., 2008. Mantle lithosphere delamination driving plateau uplift and synconvergent extension in eastern Anatolia, *Geology,* **36**(9), doi:10.1130/G24982A.1, 723-726.

Gök, R., Sandvol, E., Türkelli, N., Seber, D. & Barazangi, M., 2003. Sn attenuation in the Anatolian and Iranian plateau and surrounding regions, *Geophys. Res. Lett.,* **30**(24), 8042, doi:10.1029/2003GL018020.

Hearn, T.M., 1984. *Pn* traveltimes in Southern California, *J. geophys. Res.,* **89**(B3), 1843–1855.

Hearn, T.M., 1996. Anisotropic *Pn* tomography in the western United States, *J. geophys. Res.,* **101**(B4), 8403–8414.

Hearn, T.M. & Ni, J.F., 1994. *Pn* velocities beneath continental collision zones: the Turkish-Iranian Plateau, *Geophys. J. Int.,* **117,** 273–283.

Kaymakci, N., Duermeijer, C.E., Langereis, C., White, S.H. & Van Dijk, P.M., 2003. Palaeomagnetic evolution of the Cankiri Basin (central Anatolia, Turkey): implications for oroclinal bending due to indentation, *Geol. Mag.,* **140**(3), 343–355.

Keskin, M., 2003. Magma generation by slab steepening and breakoff beneath a subduction-accretion complex: An alternative model for collision-related volcanism in Eastern Anatolia, Turkey, *Geophys. Res. Lett.,* **30**(24), 8046, doi:10.1029/2003GL018019.

Keskin, M., Can Genç, S. & Tüysüz, O., 2008. Petrology and geochemistry of post-collisional Middle Eocene volcanic units in North-Central Turkey: evidence for magma generation by slab breakoff following the closure of the Northern Neotethys Ocean, *Lithos,* **104,** 267–305.

Koch, M., 1992. Bootstrap inversion for vertical and lateral variations of the S wave structure and the v_p/v_s-ratio from shallow earthquakes in the Rhinegraben seismic zone, Germany, *Tectonophys,* **210,** 91–115.

Kocyigit, A. & Beyhan, A., 1998. A new intracontinental transcurrent structure: the Central Anatolian Fault Zone, Turkey, *Tectonophys,* **284,** 317–336.

Kürüm, S., Önal, A., Boztug, D., Spell, T. & Arslan, M., 2008. $^{40}Ar/^{39}Ar$ age and geochemisty of the post-collisional Miocene Yamadag volcanics in the Arapkir area (Malatya Province), eastern Anatolia, Turkey, *J. Asian Earth Sci.,* **33,** 229–251.

Lei, J. & Zhao, D., 2007. Teleseismic evidence for a break-off subducting slab under Eastern Turkey, *Earth planet. Sci. Lett.,* **257,** 14–28.

Okay, A.I. & Tüysüz, O., 1999. Tethyan sutures of northern Turkey, in *The Mediterranean Basins; Tertiary Extension within the Alpine Orogeny,* Vol. 156, pp. 475–515, Geological Society Special Publications.

Paige, C.C. & Saunders, M.A., 1982. ALGORITHM 583 LSQR: Sparse Linear Equations and Least Squares Problems, *ACM Trans. Math. Software,* **8**(2), 195–209.

Reilinger, R. *et al*., 2006. GPS constraints on continental deformation in the Africa-Arabia-Eurasia continental collision zone and implications for the dynamics of plate interactions, *J. geophys. Res.,* **111,** B05411, doi:10.1029/2005JB004051.

Sandvol, E., Turkelli, N. & Barazangi, M., 2003. The Eastern Turkey Seismic Experiment: the study of a young continent-continent collision, *Geophys. Res. Lett.,* **30**(24), 8038, doi:10.1029/2003GL018912.

Sengör, A.M.C. & Yilmaz, Y., 1981. Tethyan evolution of Turkey: a plate tectonic approach, *Tectonophys,* **75,** 181–241.

Sengör, A.M.C., Özeren, S., Genç, T. & Zor, E., 2003. East Anatolian high plateau as a mantle-supported, north-south shortened domal structure, *Geophys. Res. Lett.,* **30**(24), 8045, doi:10.1029/2003GL017858.

Sengör, A.M.C., Tüysüz, O., Imren, C., Sakinç, M., Eyidogan, H., Görür, N., Le Pichon, X. & Rangin, C., 2005. The North Anatolian Fault: a new look, *Annu. Rev. Earth planet. Sci.,* **33,** 37–112.

Tapponnier, P., 1977. Evolution tectonique du système alpin en Méditerranée: poinçonnement et écrasement rigide-plastique, *Bull. Soc. Geol. Fr.,* **19**(3), 437–460.

Wessel, P. & Smith, W.H.F., 1998. New, improved version of the Generic Mapping Tools released, *EOS, Trans., Am. Geophys. Un.,* **79,** 579.

Whitney, D.L., Teyssier, C. & Heizler, M.T., 2007. Gneiss domes, metamorphic core complexes, and wrench zones: thermal and structural evolution of the Nigde Massif, central Anatolia, *Tectonics,* **26,** doi:10.1029/2006TC002040.

SUPPORTING INFORMATION

Additional Supporting Information may be found in the online version of this article:

Figure S1. Standard deviation of the cell velocity for each cell. Solution variances calculated using the bootstrap method with 100 iterations (Koch 1992; Hearn 1994). The average standard deviation of the velocity perturbations is 0.05 km s^{-1}.

Figure S2. (A) Crustal station delays. Average negative delay is −0.31 s; average positive delay is 0.27 s. (B) Standard deviation of the station delays for Turkey, calculated using the bootstrap method. Average error is 0.19 s. Station locations are marked with crosses, circles or squares indicate magnitude of the delay/error.

Please note: Wiley–Blackwell are not responsible for the content or functionality of any supporting materials supplied by the authors. Any queries (other than missing material) should be directed to the corresponding author for the article.